

Fast and low power Michelson interferometer thermo-optical switch on SOI

Junfeng Song^{1,2*}, Q. Fang¹, S. H. Tao¹, T. Y. Liow¹, M. B. Yu¹, G. Q. Lo¹, and D. L. Kwong¹

¹*Institute of Microelectronics, Agency for Science, Technology and Research,
11 Science Park Road, Science Park II, Singapore 117685*

²*State Key Laboratory on Integrated Opto-electronics, College of Electronic Science and Engineering,
Jilin University, 119 Jiefang Road, Changchun 130023, China*

*songjf@ime.a-star.edu.sg
<http://ime.a-star.edu.sg/>

Abstract: We designed and fabricated silicon-on-insulator based Michelson interferometer (MI) thermo-optical switches with deep etched trenches for heat-isolation. Switch power was reduced ~20% for the switch with deep etched trenches, and the MI saved ~50% power than that of the Mach-Zehnder interferometer. 10.6 mW switch power, ~42 μ s switch time for the MI with deep trenches, 13.14 mW switch power and ~34 μ s switch time for the MI without deep trenches were achieved.

©2008 Optical Society of America

OCIS codes: (250.0250) Optoelectronics; (130.0130) Integrated optics; (130.3120) Integrated optics devices; (230.3990) Microstructure devices; (220.4000) Microstructure fabrication.

References and links

1. R. Soref, "The Past, Present, and Future of Silicon Photonics," *IEEE J. Sel. Top. Quantum Electron.* **12**, 1678-1687 (2006).
2. B. Jalali, and S. Fathpour, "Silicon Photonics," *J. Lightwave Technol.* **24**, 4600-4615 (2006).
3. T. Tsuchizawa, K. Yamada, H. Fukuda, T. Watanabe, S. Uchiyama and S. Itabashi, "Low-Loss Si Wire Waveguides and their Application to Thermo-optic Switches," *Jpn. J. Appl. Phys.* **45**, 6658-6662 (2006).
4. R. L. Espinol, M.-C. Tsai, James T. Yardley, and R. M. Osgood, Jr., "Fast and Low-Power Thermo-optic Switch on Thin Silicon-on-Insulator," *IEEE Photon. Technol. Lett.* **15**, 1366-1368 (2003).
5. T. Chu, H. Yamada, S. Ishida and Y. Arakawa, "Compact $1 \times N$ thermo-optic switches based on silicon photonic wire waveguides," *Opt. Express* **13**, 10109-10114 (2005).
6. F. Gan, T. Barwicz, M. A. Popović, M. S. Dahlem, C. W. Holzwarth, P. T. Rakich, H. I. Smith, E. P. Ippen and F. X. Kärtner, "Maximizing the Thermo-Optic Tuning Range of Silicon Photonic Structures," *Optical Switch 2007 IEEE*, (San Francisco, 2007), pp.153-154.
7. M. Harjanne, M. Kapulainen, T. Aalto, and P. Heimala, "Sub- μ s Switching Time in Silicon-on-Insulator Mach-Zehnder Thermo-optic Switch," *IEEE Photon. Technol. Lett.* **16**, 2039-2041 (2004).
8. M. W. Geis, S. J. Spector, R. C. Williamson, and T. M. Lyszczarz, "Submicrosecond Submilliwatt Silicon-on-Insulator Thermo-optic Switch," *IEEE Photon. Technol. Lett.* **16**, 2514-2516 (2004).
9. T. Chu, H. Yamada, S. Ishida, and Y. Arakawa, "Thermo-optic Switch Based on Photonic-Crystal Line-Defect Waveguides," *IEEE Photon. Technol. Lett.* **17**, 2083-2085 (2005).
10. L. Gu, W. Jiang, X. Chen, and R. T. Chen, "Thermooptically Tuned Photonic Crystal Waveguide Silicon-on-Insulator Mach-Zehnder Interferometers," *IEEE Photon. Technol. Lett.* **19**, 342-344 (2007).
11. I. Kiyat, A. Aydinli, and N. Dagli, "Low-Power Thermo-optical Tuning of SOI Resonator Switch," *IEEE Photon. Technol. Lett.* **18**, 364-366 (2006).
12. M. W. Pruessner, T. H. Stievater, M. S. Ferraro, and W. S. Rabinovich, "Thermo-optic tuning and switching in SOI waveguide Fabry-Perot microcavities," *Opt. Express* **15**, 7557-7563 (2007).
13. S.-L. Tsao and P.-C. Peng, "An SOI Michelson Interferometer Sensor with Waveguide Bragg Reflective Gratings for temperature monitoring," *Microwave Opt. Technol. Lett.* **30** 321-322 (2001).
14. E. Dulkeith, F. Xia, L. Schares, W. M. J. Green, and Y. A. Vlasov, "Group index and group velocity dispersion in silicon-on-insulator photonic wires," *Opt. Express* **14**, 3853-3863 (2006).

1. Introduction

High density, compact size, low power consumption, multi-functional integrated optical devices are required for future cost-effective optical network. Since silicon-on-insulator (SOI) based silicon wire waveguide provides a very high refractive index contrast and strong light

confinement, this ultra small size and sharp bend can be realized for compact photonic circuit [1-3]. Furthermore, leveraging on mature Si-CMOS technology, ultra-compact and complex electronic controlled electro-optic devices can be expected. Because thermo-optic (TO) coefficient of Si is about tenfold larger than that of silica. Therefore, the Si-based TO switch can be expected to significantly reduce the power consumption for switching operations.

Mach-Zehnder interferometer (MZI) is widely applied for modulator, switch, and VOA. There are reports on the MZI thermal-optic switches [3-6]. Harjanne *et al.* [7] reported an SOI thermo-optic MZI with sub-microsecond switch using a two differential heaters, one on each arm of a MZI and pulse shaping the voltage across the heaters. Geis *et al.* [8] used doped silicon waveguide, which was heated directly by passing current. The switch power and time were remarkably low. Recently, the photonic crystal (PhC) based MZI TO-switches were studied [9, 10]. In addition, cavity structures, e. g., racetrack resonator [11], and Fabry-Perot micro-cavities, were applied [12].

Typically, an MZI structure consists of two splitters (1×2 or 2×2) and two arms. A Michelson interferometer (MI) is a folded MZI with similar function. The MI has only one splitter and half-length arms. Since light shuttles in the arms and the length of the tuning region is shorter (by half) than that of the MZI, thus a lower operating power can be expected for MI configuration.

In this paper, we investigate Si wire-based MI structures functioning as thermo-optic switch. The deep trench was incorporated. As reference, the MZI structures were fabricated and compared in aspect of the switch power with that of MI. In section 2, we introduce the MI structure with a mirror made of silicon wire loop, and in section 3, we describe the fabrication process. We will present the measurement results in section 4, and the conclusion is drawn in section 5.

2. MI Structure on SOI

The schematic layouts of the MZI and MI are shown in Fig. 1. The MZI in Fig. 1(a) composes of two 2×2 directional couplers (DCs) and two arm waveguides. The MI structure is shown in Fig. 1(b). In Fig. 1(a), the MZI is cut along the dashed line. Thus, mirrors at the facets of the cut waveguides are needed to reflect the lights. Although grating is a choice [13], but it works only for a very *narrow* bandwidth. To overcome this shortcoming, we adopt an optical waveguide loop as mirror, which is a *full* band reflector. The whole structure is shown in Fig. 1(c). Since the MI structure is a folded MZI structure, the light in terminal-A in the MZI (see Fig. 1(a)) will be the reflected light at the input port (see Figs. 1(b)-1(c)). Thus, the modulating length is shortened by half. The benefits of shortened modulating length are low operating power and high modulating frequency.

The MZI and MI structures are typically with equal arms, shown in Fig. 1. But in following discussion, we will use the unequal arms to demonstrate the device operation. The reason is given below. Commonly, the phase variation is described as $\Delta\phi = \Delta n k_0 L_{th}$, and for silicon, $\Delta n = 1.86 \times 10^{-4} \Delta T$, where ΔT is the temperature variations. Presumably, ΔT is directly proportional to the electric power applied on the heater. In the interferometer with unequal arms, $\Delta\phi$ is directly proportion to Δf , which is the variations of destructive interference frequency. The destructive interference frequency can be estimated from spectrum accurately. We can get the relation $\Delta f = \alpha \Delta W$, where ΔW is the power on the heater. Measuring multiple points of Δf and ΔW and by linear fitting of both, we can get coefficient α . Switch on/off states are defined as $\Delta\phi = \pi$ or $\Delta f = \text{FSR}/2$. Thus the switch power is $\text{FSR}/2\alpha$, where FSR is the free spectral region.

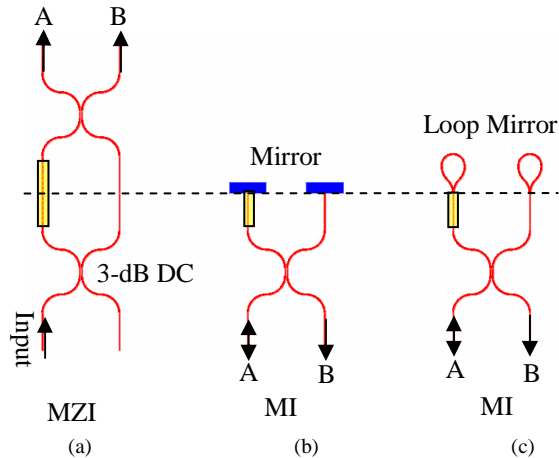


Fig. 1. Schematic layouts of 2×2 MZI and MI structures. (a) is a typical directional coupler MZI structure; (b) is a typical MI structure, where the blue boxes denote the mirrors; (c) the MI structure on SOI. Two loop waveguides are used, instead two mirrors. The yellow region denotes the modulating region.

3. Fabrication

We started the fabrication on a commercial available 200-mm SOI wafer with 400-nm-thick top silicon and 2- μm -thick buried dioxide. Top silicon was thinned down to 200 nm by oxidation. 248-nm deep UV lithography was used to define the device pattern. Inductively coupled plasma etching system was used to dry etch the silicon layer. Mosaic SEM pictures of an MI structure are shown in Fig. 2(a). The MI structure has unequal arms: one is 110 μm long and the other is 10 μm . The balloon-like waveguide loop circuit is shown in Fig. 2(b). It composes of a semicircle and two S-shape waveguides. The diameter of the semicircle is 23.5 μm , and the length of the S-curve is 28 μm . The 3-dB DC is 11 μm long, the gap of two waveguides is 0.3 μm , and waveguide widths are the same as 0.4 μm . The SEM picture is shown in Fig. 2(c). Spot size converters (SSCs) were integrated on the input and output terminals. The SSC is a 200- μm long taper with 200-nm wide tip.

After deposition of 1 μm high-density plasma (HDP) oxide, 100 nm Titanium is deposited. Titanium is selected as the heater metal for its high electrical resistance and heat resistance. UV lithography is applied again to define the heater pattern on the Titanium. The heater is etched as saw-like shape to increase the electrical resistance. The arm and 3-dB DC heaters are shown in Figs. 2(d) and 2(e). The lengths of the arm- and DC- heater are 100 μm and 9 μm , respectively. The width of the Titanium wire is 500 nm and the gap between the wires is also 500 nm. Then, 1 μm HDP oxide was deposited. After the contact holes formation, 750 nm Aluminum was deposited. The final process was the deep trench etch. The deep trench is a 3 μm -wide groove. The groove edge is 3 μm away from the waveguide and 2 μm away from the metal (heat or pad). The deep trench will be used to prevent heat diffusion. The depth of the groove is \sim 100 μm . The groove is for the heat isolation, but do not need so deep. \sim 100 μm depth is for easier fiber coupling. The SEM picture of a coupling terminal is shown in Fig. 2(f), where an SSC is enclosed. The tip of the SSC is 3 μm away from the coupling facet. The micrograph picture of the final device is shown in Fig. 2(g). The dark round strip device is the deep etched groove. For comparison, an MZI structure was fabricated on the same wafer [shown in Fig. 2(h)]. The optical delay line is made as clip shape [14] such that the length difference can be controlled accurately. In our device, the length difference is 200 μm , two times of that of the MI. The MZI heater is two times as long as the MI one, too. Total device length is 2.9 mm.

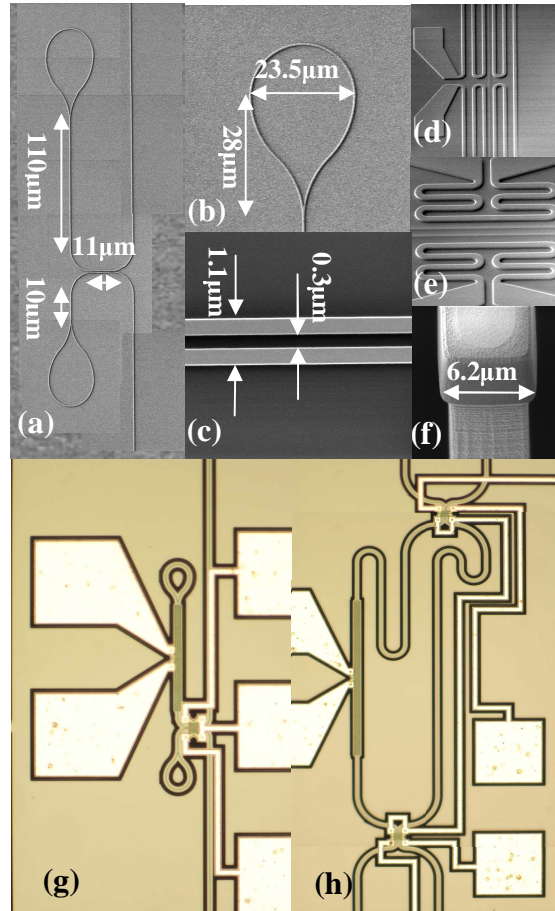


Fig. 2 (a) is SEM picture of a full MI structure after silicon etching. The two arms are 110 μm and 10 μm long, respectively. The length of the 3-dB DC is 11 μm . (b) is the loop silicon wire. The top is a semicircle with diameter of 23.5 μm . The length of the two S-shape curves is 28 μm . (c) is the gap of the 3-dB DC. The gap width is 0.3 μm and the waveguide width is 0.4 μm . (d) is the arm heater pattern. (e) is 3-dB DC heater pattern. The heater wire is 0.5 μm wide and the gap is 0.5 μm . (f) is SEM picture of coupling section with fiber. (g) is microscope picture of the MI structure. (h) is microscope picture of the MZI structure.

4. Results and discussions

Firstly, we measured the electric-resistance of the arm heater to be 16.625 k Ω . The electric-resistance is very high, so that, we can assume that all of the electric power is on the heater. The cross-section and length of the heater is 0.1 $\mu\text{m} \times 0.5 \mu\text{m}$ and $\sim 600 \mu\text{m}$, respectively, we can estimate the electrical resistivity as $\sim 138 \mu\Omega\text{-cm}$, which is ~ 7.34 times of that of bulk Titanium.

The transmission measurement system setup is illustrated in Fig. 3. The light source is a tunable laser or ASE (Amplified Spontaneous Emission). We tune the polarization controller (POL) to make the input light as quasi-TE mode (electric field parallel to substrate plane). The insertion loss (IL) is recorded as the fiber to fiber loss, which includes the device transmission loss and coupling loss between a fiber and a SSC. Two lensed polarization-maintaining fibers are coupled with the input and the output terminals, respectively. Firstly, the POL's IL is measured and saved as reference for the following measurements. Then, we deduct the polarization IL from the following characterization.

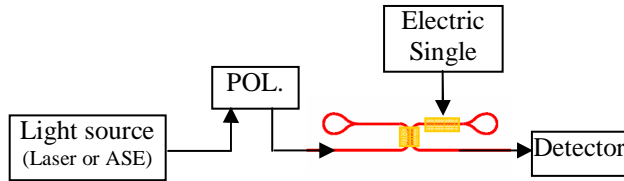


Fig. 3. The sketch map of the measurement setup. POL.: polarization controller;

4.1 Switch power of the MI structure

Because we adopt unequal lengths for two arms, the spectrum is a periodically sinusoidal curve. From the period length, we can obtain the group refractive index as 4.36 and FSR as 356.53 GHz for the deep trench device. Figure 4(a) is transmission spectra with different electric powers on the arm heater. The wavelength was fixed between 1520 and 1555 nm. The electric power was increased from 0 to 16 mW with 2 mW step. The IL is ~ 8 dB and the extinction ratio is ~ 30 dB. The destructive interference wavelength tends to red-shift with the increasing power. Figure 4(b) shows the relation of destructive frequency (the wavelength of destructive interference is translated to frequency) as function of the applied power. The blue circles denote the experimental data, and the red line is the linear fitting curve, whose slope is -0.0168 . This means that 1 mW electric power will shift 16.8 GHz frequency. The FSR has 2π phase difference, but for switch we need phase change π only, which is corresponding to 178.26 GHz. The switch power of our device is 10.6 mW.

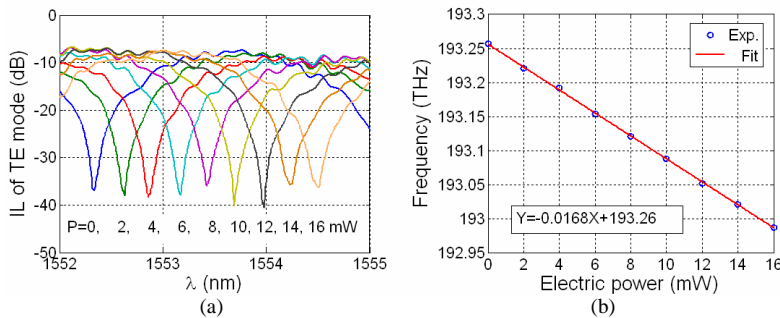


Fig. 4. Deep trench MI structure. (a). The transmission spectra with different electric power. Wavelength is from 1552 nm to 1555 nm, and electric power is from 0 to 16 mW by step 2 mW. (b). The destructive frequency as a function of electric power. The blue circles are experiment data, and the red line is fitting line.

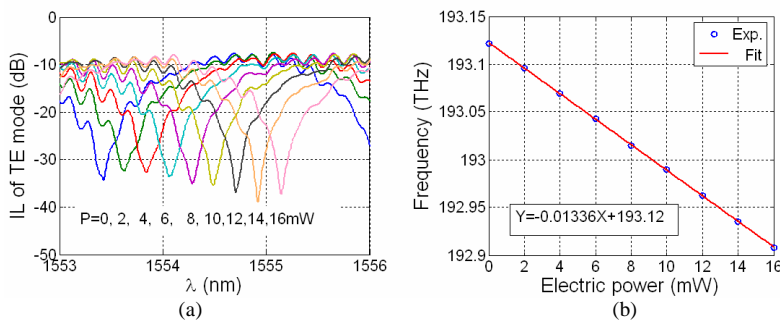


Fig. 5. The MI structure without deep trenches. (a) The transmission spectra with different electric powers. Wavelength is from 1553 nm to 1556 nm, and electric power is from 0 to 16 mW by step 2 mW. (b) The destructive frequency with electric power. The blue circles are experiment data, and the red line is fitting line.

For comparison of devices with and without deep trenches, the corresponding results without deep trench are shown in Figs. 5(a) and 5(b). The FSR is 351.08 GHz (Fig. 5(a)), and 13.36 GHz per mW (Fig. 5(b)). The switch power without deep trench is 13.14 mW. This means that the deep trench will save 19.3% operating power.

For comparison purpose, we use the same methodology to characterize the MZI structures with and without deep trenches. Figures 6(a) and 6(b) are the results of the MZI structure with deep trench. The FSR is 345.34 GHz, the heater is 8.948 GHz/mW, and the switch power is 19.3 mW. Figures 7(a) and 7(b) are the results of the MZI structure without deep trench. The FSR is 346.65 GHz, the heater is 6.648 GHz/mW, and the switch power is 26.072 mW. Thus, the structure with deep trench saves ~26% power.

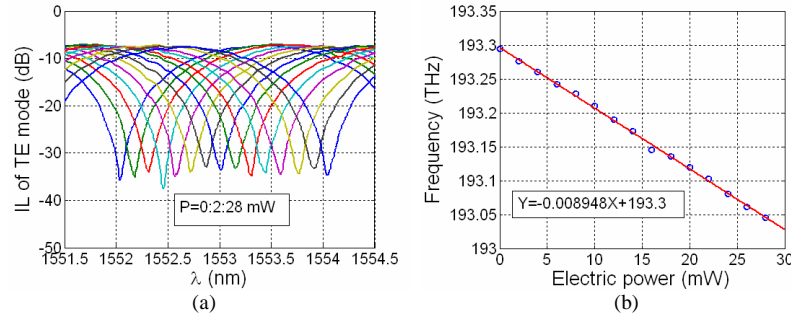


Fig. 6. The MZI structure with deep trench. (a). The transmission spectra with different electric powers. Wavelength is from 1551.5 nm to 1554.5 nm, and electric power is from 0 to 28 mW by step 2 mW. (b). The destructive frequency versus electric power. The blue circles are experiment data, and the red line is fitting line.

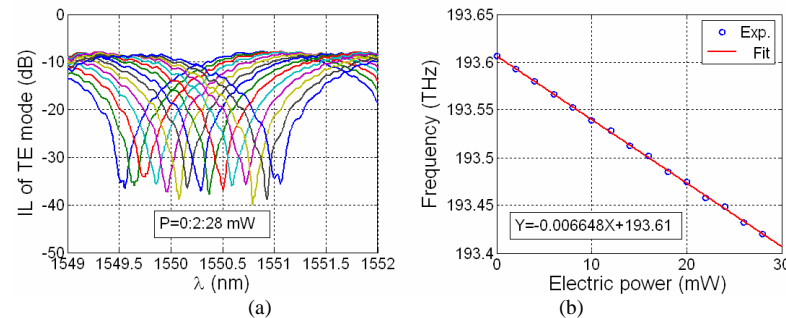


Fig. 7. The MZI structure without deep trench. (a) The transmission spectra with different electric powers. Wavelength is from 1549 nm to 1552 nm, and electric power is from 0 to 28 mW by step 2 mW. (b) The destructive frequency versus electric power. The blue circles are experiment data, and the red line is fitting line.

4.2 Switch time of MI structure

To characterize the switch speed, we replaced the ASE light source with a 1.55 μm laser and tune the POL to output in quasi-TE mode. Output light was contacted with power meter (Newport 2832-C). We scanned the transmission power by varying electric voltage on the arm to choose an optimum static working state. The results are shown in Fig. 8(a). The output light power is normalized. The voltages corresponding maximum and minimum output states are 12.6 V and 17.5 V, respectively. The extinction ratio is ~25 dB. A square-wave electric signal (HP 33250A) amplitude 5 V (maximum of amplitude) and external bias 12.6 V is used. The detector is changed as a high speed (>1 GHz) InGaAs photo-detector. The averaged rise time is 10.9 μs and the fall time is 34.9 μs , as shown in Fig. 8(b). The situations without deep trench are shown in Figs. 9(a) and 9(b), and the voltages of the maximum and minimum outputs are 7.3 and 15.9 V, respectively. We chose the bias voltage 11 V and amplitude 5 V. It

is can be seen from Fig. 7(c), 11 V voltage is close to maximum output states. The switch time is shown in Fig. 9(b). The average rise- and fall- times are 10.6 and 23.2 μs , respectively. Thus, the structure without deep trench shortens the switch time from $\sim 45.8 \mu\text{s}$ to $\sim 33.8 \mu\text{s}$, which is almost 26% shorter. The reason is that, the structures without deep trenches have better heat conduction.

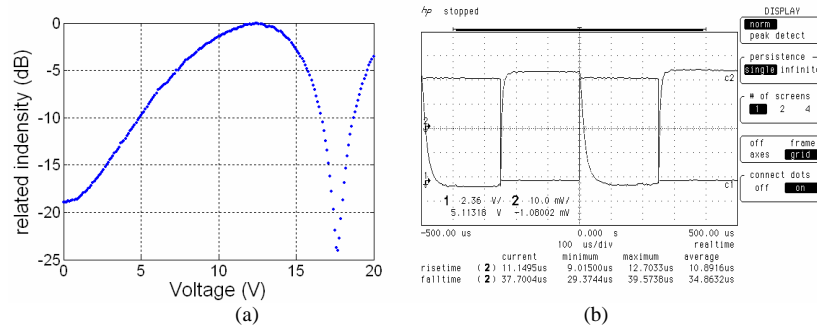


Fig. 8. The MI structure with deep trench. (a). Related intensity of output power versus static voltage. (b). Waveforms of electric signal and optical response. The rise- and fall- time are 10.9 μs and 34.9 μs , respectively.

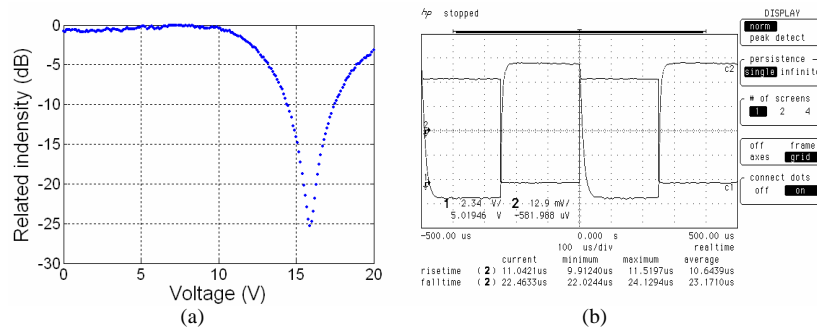


Fig. 9. The MI structure without deep trench. (a) Related intensity of output power versus static voltage. (b) Waveforms of electric signal and optical response. The rise- and fall- time are 10.6 μs and 23.2 μs , respectively.

Table 1. Recent silicon based thermo-optical switches

Year	Author	Optical structure	Switch power (mW)	Switch time (μs)	
				rise	fall
2003	Espinol [4]	MZI	50	3.5	3.5
2004	Geis[8]*	MZI	6	0.6	0.6
2004	Harjanne [7]**	MZI	-	<1	<1
2005	Chu [5]	MZI	90	<100	
2005	Chu [9]	MZI (PhC)	120	120	
2006	Tsuchizawa [3]	MZI	30	200	
2007	Gan [6]	MZI	-	7	14
2007	Gu [10]	MZI (PhC)	78	19.6	11.4
2008	This work	MZI	DT	19.3	-
		WODT	26.1	-	
2008	This work	MI	DT	10.6	34.9
		WODT	13.14	10.6	23

DT: deep trench; WODT: without deep trench;

*: Special heater (doped silicon waveguide); **: Special signal (pulse shaping)

It can be seen from the above comparison that the MI structure saves ~50% switch power more than the MZI. The MI structure benefits from the mirror structure which doubles the optical path length. And the deep trench of MI and MZI saves ~19% and 26% switch power, respectively. The structures without deep trenches have better heat conduction and thus shorter switch time, but at the expense of higher switch power. Table 1 lists the results comparing ours and the most recently reported works.

We can see that the rise time and fall time are asymmetric, due to the nature of heat conductance of devices. A low heat conductance will reduce the rise time and increase the fall time. However, for small size device, as the heater being close to waveguide, the rise time is less influenced by the heat conductance. As in the case of MI experiment, with deep trench structure (low heat conductance), the device has longer fall time (from 34.9 μ s to 23 μ s), but closed rise time (10.9 μ s and 10.6 μ s).

5. Conclusion

We have designed, fabricated, and measured the MI and MZI thermo-optical switches based on silicon wires on SOI, and compared the structures with and without deep trenches. 10.6 mW switch power, ~42 μ s switch time for the MI with deep trenches, 13.14 mW switch power and ~34 μ s switch time for the MI without deep trenches were achieved. The MIs save ~50% power more than the MZIs, and the switch power is reduced ~19% with the MI with deep etched trenches. However, the MI structure will arouse reflection when the device is on the on/off states (see Figs. 1(b) and 1(c)). On the other hand, this characteristic can be used as tunable reflector applied for Q-switch lasers.